

On the usefulness of supervised learning for vessel border detection in IntraVascular Imaging

Aura Hernández ^{a,1}, Debora Gil ^a & Petia Radeva ^{a,b}

^a *Centre de Visió per Computador*

^b *Dept. de Ciències de la Computació UAB*

Abstract. IntraVascular UltraSound (IVUS) imaging is a useful tool in diagnosis of cardiac diseases since sequences completely show the morphology of coronary vessels. Vessel borders detection, especially the external adventitia layer, plays a central role in morphological measures and, thus, their segmentation feeds development of medical imaging techniques. Deterministic approaches fail to yield optimal results due to the large amount of IVUS artifacts and vessel borders descriptors. We propose using classification techniques to learn the set of descriptors and parameters that best detect vessel borders. Statistical hypothesis test on the error between automated detections and manually traced borders by 4 experts show that our detections keep within inter-observer variability.

Keywords. classification, vessel border modelling, IVUS

1. Introduction

Intravascular UltraSound is a helpful clinical tool [1] to diagnosis and treatment of cardiac diseases since images assist cardiologists to achieve a complete study of vessel morphology, such as, arterial wall, plaque or lumen. Segmentation of vessel borders is a common processing in intravascular imaging that allows plaque quantification or estimation of stenosis for instance. However, manual segmentation is a tedious and time consuming task, so different techniques addressed to the semi-automatic and automatic segmentation have been developed along early years. Furthermore, by its inherent difficulty (its distance from the transducer reduces sharpness in the border visual appearance), adventitia modelling has been only approached in recent works ([5]-[8]). In this article we present a novel strategy for detection of the most external vessel border, the adventitia layer.

Most approaches ([2]-[8]) are based on deterministic principles. However, poor quality of images as well as large variety of descriptors and a weak appearance of the adventitia, make standard segmentation approaches difficult to achieve proper results by their own. This implies additional specific techniques such as combining transversal and

¹Correspondence to: Aura Hernández, Edifici O, Campus UAB, 08193 Bellaterra, Barcelona, Catalonia, Spain. Tel.: +34 935 812 301; Fax: +34 935 811 670; E-mail: aura@cvc.uab.es.

longitudinal cuts ([2]-[3],[7]-[9]), or handling raw data [4]. Other authors ([4]-[6],[10]) use classification techniques as a robust way to noise and artifacts. However, classification strategies are usually focused on discrimination and classification rather than a segmentation problem, so adventitia is detected as a side result of plaque classification.

We agree in using classification strategies but oriented to learn the parameters that yield the optimal segmentation of vessel borders comparing with manual models, i.e., that achieve minimum error distances. Segmentation procedures can be considered as a two-fold algorithm consisting in a extraction of points laying on the adventitia and a recovery of a closed model of the extracted points. In this paper, we report an exhaustive survey on parameters performance for the extraction of adventitia contours.

The topics are presented as follows. In section 2 we describe the statistical pose of the topic. Section 3 is dedicated to present the statistics of the study, both the parameter study of our training set (Subsect. 3.1) and, validation of the method (Subsect. 3.2). Finally, section 4 discuss the conclusions and further work.

2. A Statistical Posing of the Topic

The strategy for adventitia border detection we follow is based on two main steps: selection of the points on vessel border and segmentation of the selected points. Since, in an IVUS plane, adventitia appears as a circular line (fig.1(a)), we simplify the process by working in polar coordinates (fig.1(b)) with the origin at the geometric center mass of a certain set of points laying on the adventitia layer [9]. We will note $I(i, j)$ the image in polar coordinates, for $i = 1, \dots, \min(Nc, Nr)$ and $j = 1, \dots, 360$, where Nc, Nr are the dimensions of the original image. Furthermore, in order to enhance vessel borders appearance in the polar transform, a Restricted Anisotropic Diffusion [12] is applied.

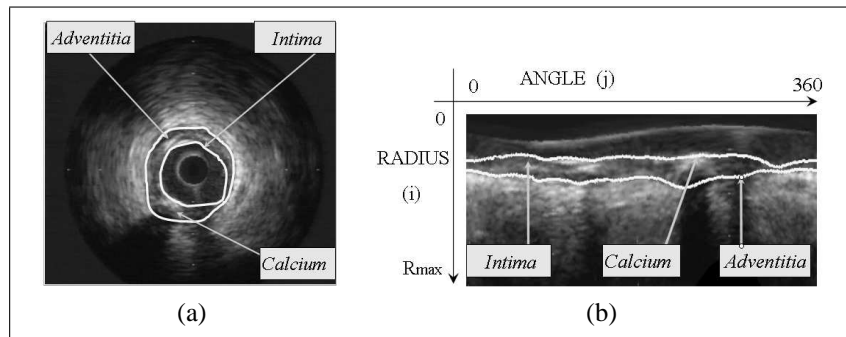


Figure 1. Main structures in an IVUS plane:cartesian domain (a) and polar transform (b).

In a segmentation procedure there are two kind of parameters. On one hand, we have to choose discriminating parameters that serve to characterize the target structures. On the other hand, we have to take into account what filtering parameters on the former response are the best for performing a proper segmentation.

For the feature space design, we assume that the intima and adventitia borders are a single class, since they are so similar and their distinct radial position serves to discriminate them [8] in the absence of echo opaque structures (EOS). In the presence of such structures, only the intima is detected, so a proper solution is to discard echo opaque

sectors by adding their characterization on the training stage. In order to avoid longitudinal cuts, we also include fibrous tissue discrimination. Two binary images are computed: vessel borders points and calcium sectors.

Filtering parameters remove spurious fake detections from the former discrimination stage. There are two main candidates to act as filtering parameters, length filtering and area filtering of the vessel borders masks. An exhaustive study determine which is the best parameter to yield, together with thresholding parameters properly tuned, an optimal segmentation of manually traced borders.

2.1. Feature space

The features that best characterize the adventitia/intima set and EOS define a three dimensional space as follows:

1. *Horizontal Edges*: In our coordinate system, vessel borders appear as nearly horizontal lines (fig.1(b)), so horizontal edges constitute our main descriptor. Then, the edges are computed by convolving the image with the y -partial derivative of a 2 dimensional gaussian kernel of variance ρ :

$$e_y(i, j) = g_y * I \quad \text{for} \quad g_y(i, j) = -\frac{j}{2\pi\rho^4} e^{-(i^2+j^2)/(2*\rho^2)}$$

The only image structures yielding large values for e_y are intima, adventitia and EOS. Intima and adventitia correspond to negative values, while EOS yield negative and positive responses, one for each of their bordering sides.

Brightness for fibrous plaque and dark shadow underneath calcium are the descriptors chosen to detect EOS and the functions measuring such features are:

2. *Radial Standard Deviation*: Brightness corresponds to an outlier of the pixel gray value in the radial distribution. We measure it by means of the difference between the pixel gray value and the radial mean. For each pixel (i, j) , we define it as

$$\sigma(i, j) = (I(i, j) - \nu(\theta))^2, \quad \text{for} \quad \nu(\theta) = \frac{1}{R_{max}} \sum_{i=1}^{i=R_{max}} I(i, \theta)$$

The radial mean of the polar image. σ is maximum at EOS and minimum near the adventitia. In order to distinguish between calcium and fibrous plaque, we add the following shadows detector:

3. *Cumulative Radial Mean*: For each angle j consider the following cumulative mean:

$$CS_j(i) = \frac{\sum_{n=R_{max}}^{n=i} I(n, j)}{R_{max} - i}$$

$CS_j(i)$ presents a sensible step for angles with calcium rather than a uniform response in the presence of fibrous plaque. It follows that the total energy:

$$ecs(j) = \sum_{i=1}^{i=R_{max}} CS_j(i)$$

achieves its minimum values only at angles with calcium.

The feature space achieving a maximum separability for our training set is given by:

$$(X, Y, Z) = (e_y, \text{sign}(e_y) \sqrt{|e_y \sigma|}, ecs)$$

2.2. Parameter choice

For the computation of the vessel borders and calcium binary images, the classification problem we must face is discriminating among 4 different sets: adventitia/intima (Adv), calcium (Cal), fibrous structures (Fbr) and the rest of pixels (RP). Instead of addressing the 4-class problem as a whole, we will solve several 2-class problems in 2 dimensions. For its simplicity, our main classifying tool will be Fisher linear discriminant analysis [13]. We will use a Bayesian approach [13] to select thresholding values in terms of miss classification errors. This is the strategy we propose for the computation of the Adv and Cal images.

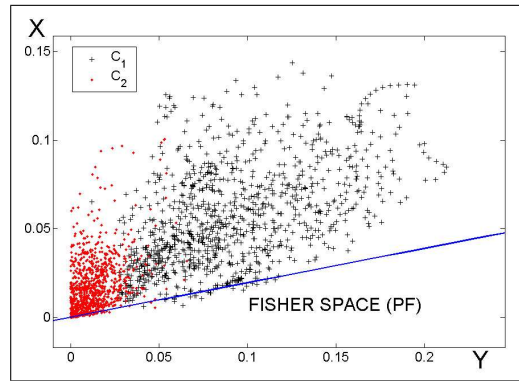


Figure 2. Adventitia vs bright structures

A. Vessel Borders Mask. Borders extraction is achieved by addressing 2 classification issues: discriminate $C_1=(Adv,RP)$ and $C_2=(Cal, Fbr)$ in the (X, Y) plane and, then, separate Adv from RP using X values. We discriminate C_1 (positives) and C_2 (negatives) by projecting onto the Fisher space, $PF1$, (see fig.2). Among all threshold ensuring a 90% of true C_1 detections, we choose the value, $TH1$, that, in combination with the rest of parameters, yields optimal segmentation results. Discrimination between Adv and RP is achieved in the X coordinate domain, as Adv corresponds to large negative values. Large range of Adv values among different patients, suggests the use of an image sensitive threshold rather than a common value for all cases. We adopt a strategy in the fashion of discriminant snakes [10] and select a different value for each angle. Radial percentiles ($PRCT_X$) are used to compute such threshold. Small structures in the vessel borders image can be removed by applying a length or an area filtering. In our case, we use a length filtering given by a certain percentile and an absolute area fixed for all frames. Although a length filtering is more flexible some 3D continuity might be lost. In contrast, an area filtering is fixed for all frames but takes into account 3D continuity.

It follows that, for every frame, points are labelled as Adv if they fulfill:

$$PF1 < TH1, X < PRCT_X \quad \text{and their length/area is above } PRCT_L.$$

B. Calcium Mask. The feature space chosen to discriminate calcium from fibrous tissue is given by the projection $PF1$ and the Z coordinate. A threshold on the Fisher space, $PF2$, for the 2D space $(PF1, Z)$ separates Cal and Fbr . Instead of following a Bayesian approach we will consider precision to select thresholding values, as we can not run the risk of identifying too much Fbr and artifacts (noise) as calcium. As in the computation of the vessel borders mask, among all thresholds admitting, at most, a 10% of noise, we choose the value, namely $TH2$, that ensures a better segmentation of our training set. That is, calcium points are those pixels that satisfy:

$$PF1 \geq TH1 \quad \text{and} \quad PF2 > TH2$$

The fragmented segments resulting from these masks are modelled by computing an Anisotropic Contour Closing [11] based on functional extension principles and then, an explicit snake representation using B-splines.

3. Results

Experiments focus on determining the best set of discriminant and filtering parameters in a training stage and assessment of the whole strategy on a test set. The sequences used have been captured with a Boston Scientific Clear View Ultra scanner at 40 MHz with constant pull-back at 0.5 mm/sec and acquisition rate of 25 frames/sec. The digitalized sequences are 384×288 images with a spatial resolution of $PixSze = 0.043500$ mm per pixel. The study group has been designed to asses the ability of the reported algorithm to detect the adventitia border in the presence of different plaques, artifacts and vessel geometries. 5400 images extracted from 11 different cases have been tested. We have segmented 22 vessel segments of a length ranging from 4 to 6 mm (200-300 frames) and including segments with uncomplete vessel borders due to side-branches and sensor guide shadows, calcified and non calcified segments and normal segments. For each segment, the adventitia has been manually traced every 10 frames by 4 experts in IVUS image interpretation, which yields a total number of 540 validated frames with 4 different manual models.

To asses segmentation accuracy, the automatically detected borders have been compared to the manual models. Accuracy is quantified by means of distance maps to manual contours, D , and difference in vessel areas, AD. We have considered absolute ($MaxD$, MD) and relative (percentage) ($RMaxD$, RMD) errors. The set of functions measuring accuracy in positions are:

- **Maximum distance errors** (in mm and %):

$$MaxD = \max_p (D(p) \cdot PixSze), \quad RMaxD = \max_p (RelD(p))$$

- **Mean distance errors** (in mm and %):

$$MD = \text{mean}_p (D(p) \cdot PixSze), \quad RMD = \text{mean}_p (RelD(p))$$

- **Percentage of Area Differences**

$$AD = 100 \cdot \frac{\sum_{i,j} |I_M(i, j) - I_A(i, j)|}{\sum_{i,j} I_M(i, j)}$$

for I_M and I_A , manual and automatical models respectively.

Table 1. Comparison of Segmenting Parameters

	$TH1 : 0.0578$ $TH2 : -0.1295$	$TH1 : 0.0619$ $TH2 : -0.1295$	$TH1 : 0.0567$ $TH2 : -0.1241$	$TH1 : 0.0567$ $TH2 : -0.01468$	$TH1 : 0.0567$ $TH2 : -0.1295$
Area 100	0.201 ± 0.046	0.201 ± 0.045	0.234 ± 0.093	0.234 ± 0.088	0.231 ± 0.089
Area 150	0.200 ± 0.045	0.200 ± 0.045	0.227 ± 0.082	0.230 ± 0.082	0.227 ± 0.081
Area 200	0.203 ± 0.045	0.220 ± 0.056	0.219 ± 0.069	0.230 ± 0.083	0.219 ± 0.069
Length 80 (%)	0.227 ± 0.060	0.199 ± 0.041	0.203 ± 0.043	0.204 ± 0.048	0.203 ± 0.043
Length 85 (%)	0.240 ± 0.070	0.237 ± 0.064	0.202 ± 0.044	0.203 ± 0.044	0.206 ± 0.048

3.1. Parameters Study

Parameter learning is performed by analyzing mean absolute segmentation errors for a training set of 6 vessel segments which are representative of all kinds of plaques and vessel morphologies. The parameters to contrast are, on one hand, filtering parameters and, on the other hand, discriminating parameters. Table 1 summarizes the statistics for the best mixtures of thresholds ($TH1$, $TH2$). It follows that the set of optimal parameters for a Boston Clear View is given by the projections:

$$PF1 = 0.1906X + 0.9817Y \quad \text{and} \quad PF2 = -0.1498PF1 + 0.9887Z$$

with the thresholds for computation of vessel borders and calcium masks set to:

$$\text{Vessel borders: } TH1 = 0.0619; PRCT_X = 6\%; PRCT_L = 80\%$$

$$\text{Calcium: } TH2 = -0.1295$$

3.2. Validation

Some of the adventitia segmentations achieved with this strategy are shown in figure 3. The first row (fig.3(a)-(d)) corresponds to images with calcified plaque (fig.3(a),(b)) and non-calcified (fig.3(c),(d)) vessel segments. Images with missing information are shown in the second row, sensor guide shadows in fig.3(e),(f) and side branches in fig.3(g)-(h).

Table 2. Statistics Summary

	NON-CALCIFIED		CALCIFIED		TOTAL	
	INT-OBS	AUT	INT-OBS	AUT	INT-OBS	AUT
MaxD (mm)	0.42 ± 0.17	0.42 ± 0.10	0.66 ± 0.36	0.71 ± 0.25	0.53 ± 0.30	0.57 ± 0.22
RMaxD (%)	0.39 ± 0.17	0.38 ± 0.10	0.54 ± 0.31	0.61 ± 0.26	0.46 ± 0.26	0.51 ± 0.23
MD (mm)	0.17 ± 0.06	0.18 ± 0.03	0.26 ± 0.13	0.28 ± 0.09	0.22 ± 0.11	0.22 ± 0.06
RMD (%)	0.16 ± 0.06	0.16 ± 0.03	0.21 ± 0.11	0.21 ± 0.11	0.18 ± 0.09	0.19 ± 0.06
AD (%)	6.67 ± 3.15	7.25 ± 1.98	9.35 ± 5.75	10.04 ± 4.03	7.98 ± 4.79	8.60 ± 3.34

In order to robustly assess the accuracy of the automated segmentations we have compared the error measures to inter-observer variability [15]. Student T-tests are used to determine if there is any statistical significant difference between inter-observer and automated distance errors. Statistical ranges (mean \pm standard deviation) for automatic errors (AUT) and inter-observer variability (INT-OBS) are summarized in table 2. We

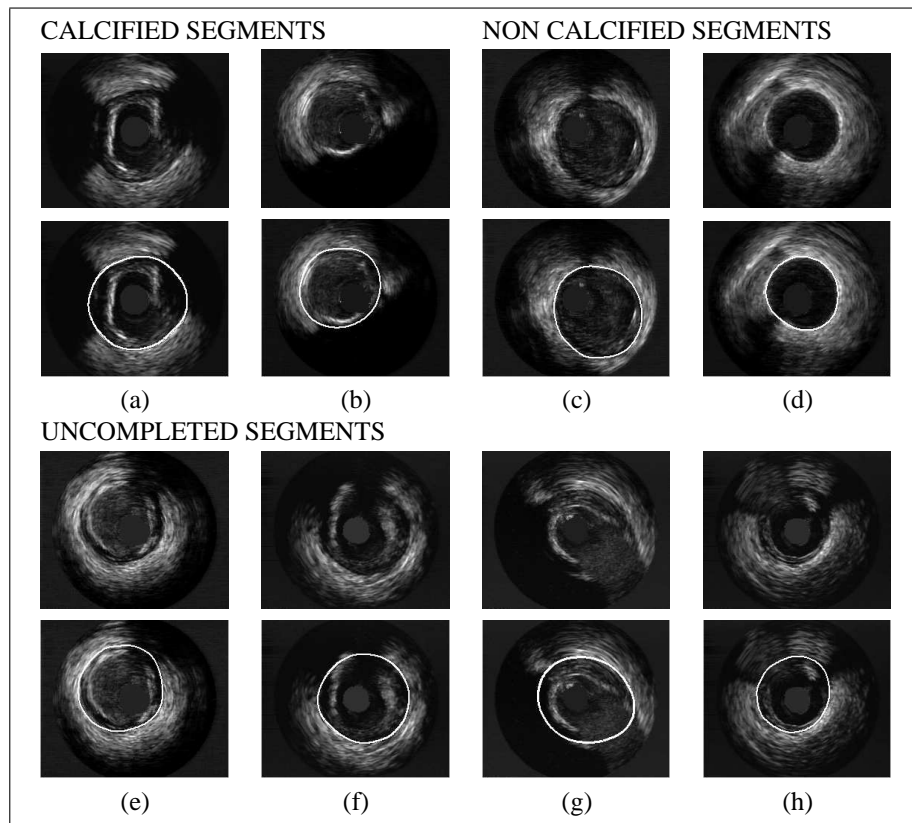


Figure 3. Automated Adventitia Detections

present statistics for non-calcified segments in the first column, calcified ones in the second and a total population of 20 vessel segments in the last column. According to a two tailed T-test, there is no significant difference between inter-observer and automated mean absolute distance errors and difference in areas. For mean distance errors the p -value equals $p = 0.177$ and the confidence interval for the true difference in means at a significance level of 95% is $CI = (-0.002, 0.014)$. In the case of percentage in area difference, $p = 0.153$ and the interval (also at a significance level of 95%) is $CI = (-0.017, 0.114)$. Although maximum errors for automated detections are lightly above the range of maximum inter-observer variability, their increase is under a 10.3%.

The fact that both mean distances and vessel areas compare to inter-observer variation validates our method for extraction of clinical measurements. Besides the number of outlier bad segmentations requiring manual correction represent less than a 15% of the studied images and, with the computing tools available, the time spend in their manual correction is in the range accepted by clinical experts.

4. Conclusions and future work

A supervised statistical survey on parameters yielding an optimal segmentation of vessel borders is presented in this paper. It shows that supervised statistical techniques are an

efficient approach to treat poor quality in intravascular imaging, as well as, large variety of descriptors such as shadows, side branches and other artifacts in IVUS images. Our segmenting strategy combines statistical techniques with deterministic principles and has been tested on 5400 images extracted from 11 different patients. Statistics show that statistical learning is a relevant tool to achieve a proper vessel borders modelling.

Nevertheless, in 16% of the cases, models are not in the range of inter-observer variability. It is mainly due to bad image acquisition and lack of image information in more than 180° because of calcium shadowing. As a result, our future work will focus on introduce a descriptor taking into account experts strategy for interpolate segments strongly lacking of information.

References

- [1] D. Hausmann, Andre J.S. Lundkvist, Guy Friedrich, Krishnankutty Sudhir, Peter J. Fitzgerald and Paul G. Yock, " Lumen and Plaque Shape in Atherosclerotic Coronary Arteries Assessed by In Vivo Intracoronary Ultrasound Beyond Angiography". *Intravascular Ultrasound: State-Of-The-Art, XX Congress of the ESC*, vol. 1, 1998.
- [2] C. von Birgelen, C. D. Mario, W. Li, J. C. Schuurbijs, C. J. Slager, P. J. de Feyter, J. R. Roelandt, and P. W. Serruys, "Morphometric analysis in three-dimensional intracoronary ultrasound: An in vitro and in vivo study performed with a novel system for the contour detection of lumen and plaque", *Amer. Heart J.*, vol. 132, pp. 516:527, 1996.
- [3] C. von Birgelen, G. S. Mintz, A. Nicosia, D. P. Foley, W. J. van der Giessen, N. Bruining, S. G. Airoian, J. R. T. C. Roelandt, P. J. de Feyter, and P. W. Serruys, "Electrocardiogram-gated intravascular ultrasound image acquisition after coronary stent deployment facilitates on-line three-dimensional reconstruction and automated lumen quantification", *J. Amer. Coll. Cardiol.*, vol. 30, pp. 436:443, 1997.
- [4] E. Brusseau, C.L. de Korte, F. Mastik, J. Schaar, Anton F. W. van der Steen, "Fully Automatic Luminal Contour Segmentation in Intracoronary Ultrasound Imaging: A Statistical Approach", *IEEE Transactions On Medical Imaging*, vol. 23, no. 5, 2004.
- [5] M. Sonka and X. Zhang and M. Siebes et al. "Segmentation of intravascular ultrasound images: A knowledge based approach", *IEEE Trans. on Medical Imaging*, 14: 719:732. 1995.
- [6] X. Zhang, M. Sonka, "Tissue characterization in intravascular ultrasound images", *IEEE Trans. on Medical Imaging*, vol. 17, no.6, pp. 889:899, 1998.
- [7] J. Dijkstra, G. Koning and J.H.C. Reiber, "Quantitative measurements in IVUS images". *The International Journal of Cardiovascular Imaging*. vol. 15, no 6, pp. 513:522, 1999.
- [8] A. Hernandez, D. Gil, P. Radeva, E. Nofrerias, "Anisotropic Processing of Image Structures for Adventitia Detection in IVUS Images", *IEEE Proc. CiC 2004*, vol. 31, pp. 229:232.
- [9] D. Gil, A. Hernandez, A. Carol, O. Rodriguez, P. Radeva, "A Deterministic-Statistic Adventitia Detection in IVUS Images", *Functional Imaging and Modeling of the Heart 2005, Barcelona, Spain, June 2-4, 2005*.
- [10] X.M. Pardo, P. Radeva, D. Cabello, "Discrimant snakes for 3D reconstruction of anatomical organs", *Medical Image Analysis*, vol. 7, pp. 293:310, 2003.
- [11] D. Gil, P. Radeva, "Extending Anisotropic Operators to Recover Smooth Shapes", *Comp. Vis. Imag. Unders.*, (in press)
- [12] D. Gil, "Geometric differential operators for shape modelling", *PhD Thesis, Universitat Autònoma de Barcelona*, 2004.
- [13] R. Duda, P. Hart, "Pattern Classification", *Wiley-Interscience*, 2001.
- [14] D.R. Martin, C.C. Fowlkes, J. Malik, "Learning to detect natural image boundaries using local brightness, color and texture cues", *IEEE PAMI*, vol. 26, pp. 1:20, 2004.
- [15] Landis JR, Koch GG, "The measurement of observer agreement for categorical data", *Biometrics*, vol. 33, pp.159:74, 1977.